LIGHT PRESSURE EFFECT ON THE ORBITAL EVOLUTION OF SPACE DEBRIS IN LOW-ORDER RESONANCE REGIONS

Eduard D. Kuznetsov, Polina E. Zakharova, Dmitry V. Glamazda, and Stanislav O. Kudryavtsev

Ural Federal University, Astronomical Observatory, Lenin ave., 51, 620000 Ekaterinburg, Russia,
Email: Eduard.Kuznetsov@usu.ru

ABSTRACT

The effect of the radiation pressure and Poynting–Robertson effect on the evolution of the orbits of satellites in low-order resonance regions is studied, depending on their area-to-mass ratio (AMR). The regions of low-order resonance zones 1:1, 1:2 and 1:3 are considered. The orbital evolution of geosynchronous, supergeosynchronous, GPS, Molniya and circular equatorial objects for resonances 1:2, 1:3 are studied from numerical simulations on period of time 240 yr and from positional observations at the SBG telescope of the Astronomical Observatory of the Ural Federal University. Secular perturbations of semi-major axes of orbits, caused by the Poynting–Robertson effect, are estimated in the region of low-order resonance zones at different AMR.

Key words: light pressure; Poynting-Robertson effect; low-order resonances; area-to-mass ratio.

1. INTRODUCTION

The orbital evolution of Earths satellites in the neighborhood of low-order resonances (1:1, 1:2, and 1:3) was studied by many authors (see, e.g., [1, 2, 8, 21]).

The problem of the motion of satellites with a high area-to-mass ratio (AMR) again became of interest after more than a hundred objects with AMR from 1 to 50 m^2/kg were identified in near-Earth space [11]. The AMR of these objects, related to space debris, is much higher than the AMR values characteristic of artificial Earth's satellites. At such high AMR values, perturbations caused by light pressure are second in value after Earths gravitational field; they are the factor affecting the motion of bodies in near-Earth space. Works devoted to the study of the light field effect on the motion of geosynchronous objects are briefly reviewed in [12].

The long-term orbital evolution of objects in the neighborhood of the 1:2 resonance was studied, for example, in [7, 3].

When studying the long-term orbital evolution of objects with a high AMR, the Poynting-Robertson effect should be taken into account. This effect leads to a secular decrease in the semi-major axis [18, 16, 19, 17, 20, 12, 14].

In this work, we present estimates of the AMR of objects moving in the neighborhood of low-order resonances obtained from the results of positional observations at the SBG telescope of the Astronomical Observatory of the Ural Federal University (AO UrFU). Based on data of numerical simulation for low-order resonances, the positions and sizes of resonance zones are defined depending on the AMR; secular perturbations of the semi-major axes of the orbits are estimated in the neighborhood of the resonance zones.

2. QUALITATIVE CHANGES OF THE ORBITAL EVOLUTION DUE TO THE RADIATION PRESSURE

The study of orbital evolution on long time intervals was performed on the basis of the results of numerical simulation. We used "A Numerical Model of the Motion of Artificial Earth's Satellites", developed by the Research Institute of Applied Mathematics and Mechanics of the Tomsk State University [5]. The model of disturbing forces taken into account the main perturbing factors: the nonsphericity of the gravitational field of the Earth (model EGM96 [15], harmonics up to the 27th order and degree inclusive), the attraction of the Moon and the Sun, the tides in the Earths body, the direct radiation pressure, taking into account the shadow of the Earth (the reflection coefficient of the satellite surface $k = 1.44$), the Poynting–Robertson effect, and the atmospheric drag. The integration of motion equations was carried out by the Everhart method of the 15th order. The specified parameters of the model provided necessary accuracy for solving the problem of motion prediction in a time interval of 240 yr [13].

2.1. Geosynchronous orbits

For the geostationary orbit, estimates of values of AMR were obtained, with which it is possible to exit the li-

bration resonance mode. In the vicinity of the stable point with initial longitude of the subsatellite point $\lambda_0 = 75°$, the exit from the libration resonance is registered at the value of the AMR γ from 5.9 to 6.0 m^2/kg ($k\gamma = 8.496 - 8.640$ m^2/kg); in the vicinity of the unstable point $\lambda_0 = 345°$, at $\gamma = 1.4 - 1.5$ m^2/kg ($k\gamma = 2.016 - 2.160$ m^2/kg). Fig. 1 shows the evolution of the longitude of the subsatellite point λ of the geosynchronous object with $\gamma = 6.0$ m^2/kg. The exit of the object from the libration resonance occurs along a quasi-random trajectory. During this process, the motion mode changes several times (the libration relative to the point with a longitude $\lambda = 75°$ of with respect to $\lambda = 345°$ and a circular mode).

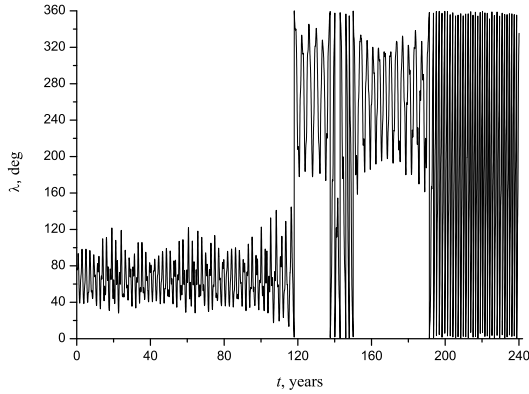*Figure 1. Evolution of the longitude of the subsatellite point λ of the geosynchronous object at the value of the AMR of $\gamma = 6$ m^2/kg.*

For initial conditions, corresponding to geosynchronous and supergeosynchronous orbits, re-entering to the Earth occurs at values of the AMR of $\gamma \geqslant 32.3$ m^2/kg ($k\gamma \geqslant 46.5$ m^2/kg), and hyperbolic exit from the Earth orbit takes place if $\gamma \geqslant 5268$ m^2/kg ($k\gamma \geqslant 7585$ m^2/kg).

With an increase in AMRs of objects, the amplitude of long- and short-period oscillations of the orbit inclination increases. The amplitude of long-period oscillations reaches 2ε (here ε is the obliquity of the ecliptic to the equator). The amplitude of short-period oscillations increases to $2°$. In the case of high AMR, maximum inclination of the orbit can reach $i = 49°$. With increasing AMR, the oscillation period of inclination is significantly reduced; i.e., from 55 years at $\gamma = 0.02$ m^2/kg to 6 years at $\gamma = 32.2$ m^2/kg.

In [6, 22] the existence of a stationary point was demonstrated in the phase plane (e_0, π_0) "eccentricity e and longitude of pericenter π", corresponding to the following initial conditions

$$e_0 \approx 0.01k\gamma, \quad \pi_0 = \lambda_\odot. \qquad (1)$$

Here $\lambda_\odot$ is the ecliptic longitude of the Sun.

With initial conditions corresponding to the stationary point (1) the mean value of the eccentricity of the orbit is retained. The amplitude of eccentricity oscillations is minimal, although it increases with the AMR. Conditions under which the solar angle is $\varphi_\odot = \pi - \lambda_\odot \approx 0$ provide a stable orbital evolution of objects with high AMR (Fig. 2).
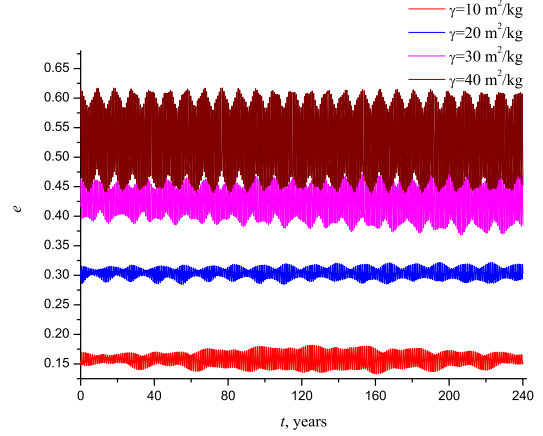

Figure 2. Evolution of the eccentricity of the orbit e of the geosynchronous object with the initial conditions corresponding to the stationary point (1).

In the vicinity of the stable point $\lambda = 75°$ the exit from the libration resonance mode occurs when the value of the AMR is from 19 to 20 m^2/kg ($k\gamma = 27.36 - 28.80$ m^2/kg). In the vicinity of the unstable point $\lambda = 345°$ the exit takes place at $\gamma = 3 - 4$ m^2/kg ($k\gamma = 4.32 - 5.67$ m^2/kg).

The re-entry of an object to the Earth is registered at values of the AMR $\gamma \geqslant 54$ m^2/kg ($k\gamma \geqslant 77.76$ m^2/kg). These values are close to the maximal values obtained in observations of estimates of AMR of geosynchronous objects [11].

The radiation pressure provides a natural cleansing of the geostationary field of objects with a high AMR. For objects that are not affected by the librational resonance perturbations due to the Poynting–Robertson effect lead to a noticeable secular decrease in the semi-major axis.

If $k\gamma \geqslant 78$ m^2/kg, the growth of the eccentricity of the orbit will lead to re-entering of the object to the Earth (or re-entry) in a few months. Further, we consider the re-entering of the object to the Earth to mean not only the re-entry, but entry into the atmosphere and the possible destruction of the object during the flight in the atmosphere.

If $k\gamma = 29 - 78$ m^2/kg, for some initial conditions the object can re-entry to the Earth. In this case, the result depends strongly on the initial values of the longitude of the subsatellite point, longitude of the pericenter of the orbit, longitude of the Sun, eccentricity, and so on.

Fig. 3 shows the evolution of the orbital semi-major axis a (Fig. 3a) and longitude of the subsatellite point λ (Fig. 3b) of the geosynchronous object at the value of the AMR of $\gamma = 40$ m²/kg ($\lambda_0 = 75°$). The initial data corresponds to the conditions (1), providing an orbital evolution with the "constant" eccentricity. On the interval $t = 50 - 65$ years the object is temporary captured into the libration resonance (Fig. 3b). During this time, the mean value of the semi-major axis of the orbit remains almost constant (Fig. 3a).
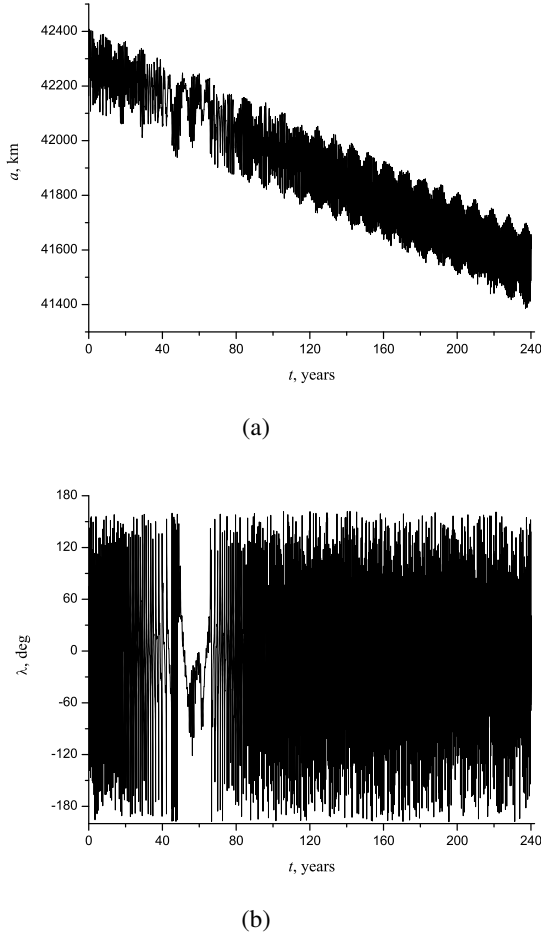

(a)

(b)

Figure 3. Evolution of (a) the semi-major axis of the orbit a and (b) longitude of the subsatellite point λ of the geosynchronous object at the value of the AMR of $\gamma = 40$ m²/kg ($\lambda_0 = 75°$). The initial data correspond to the conditions (1), providing an orbital evolution with "constant" eccentricity.

Geosynchronous objects with an initial value of the semi-major axis of the orbit $a_0 = 42165$ km with $k\gamma = 5 - 28$ m²/kg, depending on the initial conditions, can exit the libration resonance mode.

Thus a natural cleansing of the geostationary orbit occurs from the space debris with $k\gamma \geqslant 5$ m²/kg; i.e., fast

cleansing takes place on time intervals of several years for high AMR due to the influence of direct solar radiation and slow cleansing occurs at intervals up to 10^5 years for smaller values of $k\gamma$ under the influence of the Poynting–Robertson effect.

2.2. Critical arguments and their frequencies

Frequencies of perturbations caused by the effect of sectoral and tesseral harmonics of the Earth's gravitational potential are linear combinations of the mean motion of a satellite n_M, angular velocities of motion of the pericenter n_g and node n_Ω of its orbit, and the angular velocity of the Earth ω:

$$\nu_{jpq} = pn_M + jn_g + qn_\Omega - q\omega. \qquad (2)$$

The ranges of variation in the integer subscripts are $q = 1, \ldots, h$; $j = -h, \ldots, h$; $p = -\infty, \ldots, \infty$; $h = 2, \ldots, \infty$. Since the perturbation amplitudes decrease as indices increase, we are interested in conditions under which Eq. (2) is reduced to the form $\nu_{jpq} \approx 0$ at $|j|, |p|, q \leqslant 1 \div 3$.

Following [1, 2], we form the frequencies

$$\begin{aligned} \nu_1 &= u(n_M + n_\Omega + n_g) - v\omega, \\ \nu_2 &= u(n_M + n_g) + v(n_\Omega - \omega), \qquad (3) \\ \nu_3 &= un_M + v(n_g + n_\Omega - \omega) \end{aligned}$$

of three critical arguments

$$\begin{aligned} \Phi_1 &= u(M + \Omega + g) - v\omega t = \nu_1 t, \\ \Phi_2 &= u(M + g) + v(\Omega - \omega t) = \nu_2 t, \qquad (4) \\ \Phi_3 &= uM + v(g + \Omega - \omega t) = \nu_3 t, \end{aligned}$$

where M is the mean anomaly, Ω is the longitude of the ascending node, g is the argument of the pericenter, u, v are integers.

The condition $\nu_1 \approx 0$ corresponds to the resonance between the mean satellite motion n_M and the Earth's angular velocity ω (n resonance). The condition $\nu_2 \approx 0$ corresponds to an i resonance, under which the position of the ascending node of the orbit repeats periodically in a rotating coordinate system. The condition $\nu_3 \approx 0$ corresponds to a e resonance at which the position of the line of apsides is considered.

The mean longitude $l = M + \Omega + g$ is a fast variable, while the elements g and Ω are slow ones; therefore, an n resonance is a first-order resonance, and i and e resonances are second- and higher-order resonances. If there is a first-order resonance, second- and higher-order resonances can result in overlapping resonance zones and the formation of stochastic layers, where trajectory diffusion between different resonances can occur. Accounting for additional perturbations, e.g., caused by the luni-solar forces, the light pressure, and the Poynting-Robertson effect, can result in capture in resonance and escape from

the resonance of trajectories passing near the boundaries of stochasticity zone. These effects are strongest when AMR increases. The resonance structure (arrangement of resonance zones, their sizes, overlapping, etc.) of the near-Earth space for objects with high AMR, can differ significantly from a structure in which perturbations caused by the light pressure do not dominate.

2.3. Region of 1:2 resonance for circular equatorial orbits

At low AMR values $\gamma \leqslant 0.2$ m^2/kg ($k\gamma \leqslant 0.288$ m^2/kg), regions corresponding to n, i, and e resonances can be singled out in the 1:2 resonance zone. The accuracy of their boundary determination does not exceed 500 m due to the overlapping of the resonance zones.

An increase in AMR causes an decrease in the width of resonance zones. We did not succeed in separating the resonance zones for $0.2 < \gamma < 0.5$ m^2/kg ($0.288 < k\gamma < 0.72$ m^2/kg). Objects escape from the 1:2 resonance at $\gamma = 0.5$ m^2/kg ($k\gamma = 0.72$ m^2/kg). The width of the resonance zone is shown to be $\Delta a \approx 0$ km for objects with $\gamma > 0.5$ m^2/kg ($k\gamma > 0.72$ m^2/kg). This means that objects with higher AMR are in the resonance zone for a short time and then leave it.
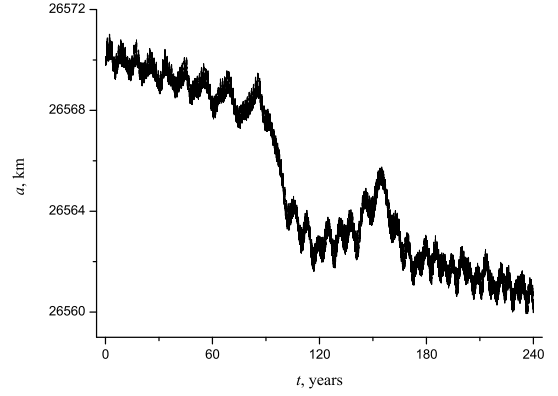
Fig. 4 and 5 show evolution of the semi-major axis of the orbit a, the eccentricity of the orbit e and the critical arguments Φ_1, Φ_2, Φ_3 of the circular equatorial object in the case of temporal capture of the object in the 1:2 resonance ($a_0 = 26570$ km, $\gamma = 0.5$ m^2/kg). Resonance passage leads to increase of the eccentricity of the orbit.

The overlapping of the resonance zones of the essential n resonance and secondary i and e resonances for circular equatorial orbits results in complex behavior of the long-term evolution of the orbit semi-major axis due to transitions between the resonance regions. The resonance zone is small, about several kilometers in size; therefore, objects with $\gamma \geqslant 0.5$ m^2/kg can escape from resonance. Again, due to an increase in the secular perturbations of the semi-major axis caused by the Poynting–Robertson effect, such objects begin to move away from the resonance zone.

2.4. Region of 1:2 resonance for GPS orbits

At low $\gamma \leqslant 0.001$ m^2/kg ($k\gamma \leqslant 0.00144$ m^2/kg), the initial values of the semi-major axis ensuring motion in the region of the 1:2 resonance coincide for n, i, and e resonances are in the range from 26558 to 26560.5 km. The amplitude of oscillations of the semi-major axis attains 14 km in the resonance zone, i.e., $a_{\min} = 26553$ km and $a_{\max} = 26567$ km.

If the initial values of the semi-major axis are outside the central part of the resonance zone ($a_0 = 26553 - 26557$,
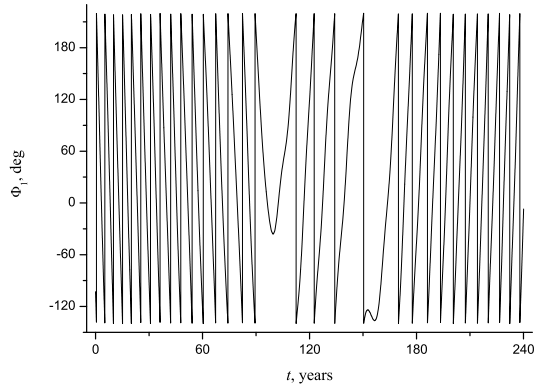
(a)
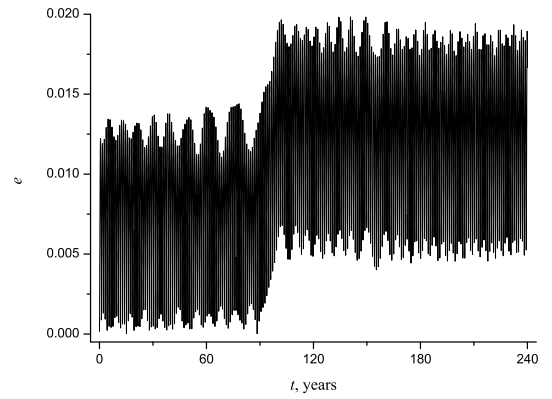
(b)

Figure 4. Evolution of (a) the semi-major axis of the orbit a and (b) the eccentricity of the orbit e of the circular equatorial object in the case of temporal capture of the object in the 1:2 resonance ($a_0 = 26570$ km, $\gamma = 0.5$ m^2/kg).

$26561 - 26567$ km), the orbital evolution remains resonant, and objects move along quasi-random trajectories. A trajectory remains in the 1:2 resonance zone, but randomly transits between different secondary resonances (Fig. 6).

In addition to n, i, and e resonances with the corresponding critical arguments Φ_1, Φ_2, and Φ_3 (4) at $u = 1, v = 2$, another two resonances are identified in this zone with the critical arguments

$$\begin{aligned} \Phi_4 &= M - \Omega + g - 2\omega t = \Phi_1 - 2\Omega, \\ \Phi_5 &= M + 2(-g + 2\Omega - \omega t) = \Phi_3 + 2\Omega - 4g. \end{aligned} \tag{5}$$
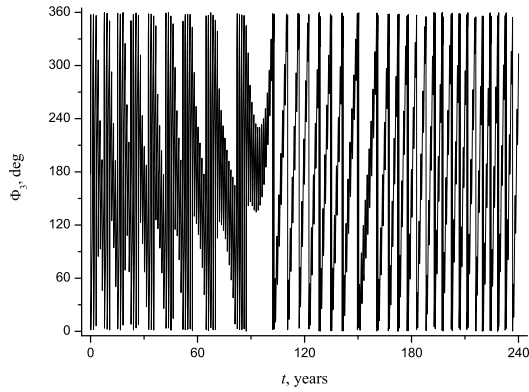
An increase in AMR results in the escape of objects from the resonance zone. The escape from the resonance zone and re-entering on long-time period is observed at $\gamma \geqslant 0.5$ m^2/kg ($k\gamma \geqslant 0.72$ m^2/kg) (Fig. 7).

(a)
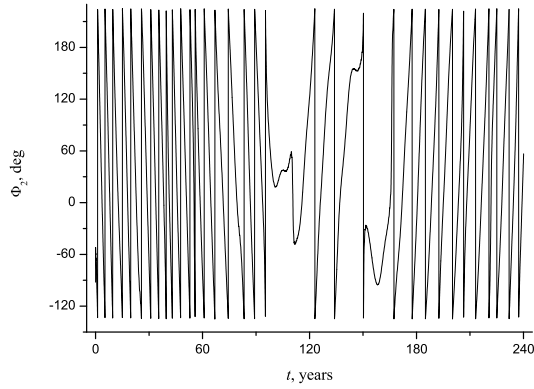
(b)

(c)

Figure 5. Evolution of the critical arguments (a) Φ_1, (b) Φ_2, (c) Φ_3 of the circular equatorial object in the case of temporal capture of the object in the 1:2 resonance ($a_0 = 26570$ km, $\gamma = 0.5$ m^2/kg).
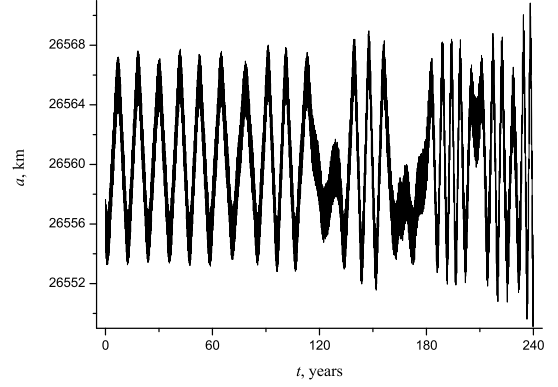

Figure 6. Evolution of the semi-major axis of the orbit a of the GPS object ($a_0 = 26557$ km, $\gamma = 0.1$ m^2/kg).
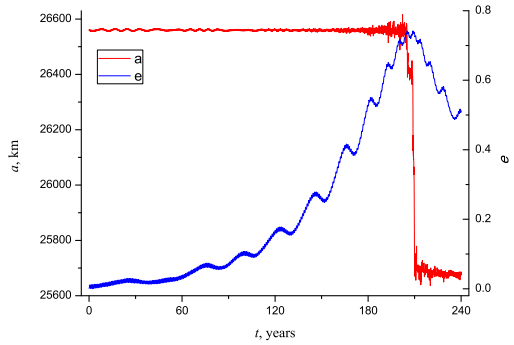

Figure 7. Evolution of the semi-major axis of the orbit a and of the eccentricity of the orbit e of the GPS object ($a_0 = 26561$ km, $\gamma = 0.5$ m^2/kg).

2.5. Region of 1:2 resonance for Molniya orbits

When determining the position and estimating the width of the 1:2 resonance zone for Molniya orbits, the initial values of the semi-major axis varied in the range $a_0 = 26480 - 26650$ km. The following initial values were used: $e_0 = 0.65$ for the eccentricity, $i_0 = 63.4°$ for the orbit inclination, and $g_0 = 270°$ for the pericenter argument.

At low $\gamma \leqslant 0.001$ m^2/kg ($k\gamma \leqslant 0.00144$ m^2/kg), the initial values of the semi-major axis ensuring motion in the region of the 1:2 resonance over 60 years were in the range from 26520 to 26522 km for an n resonance, and from 26500 to 26520 km, for i and e resonances. The amplitude of oscillations of the semi-major axis attains 60 km in the n resonance zone, i.e., $a_{\min} = 26525$ km and $a_{\max} = 26585$ km, and exceeds 100 km in zones of i and e resonances. The semi-major axis varies at least from $a_{\min} = 26470$ km to $a_{\max} = 26600$ km.

An increase in AMR in the neighborhood of the boundaries of the resonance zone results in escape from the regions of i and e resonances with transition to quasi-random trajectories passing through the regions of secondary resonances. The escape from the region of the 1:2 resonance is observed at $\gamma \geqslant 1$ m^2/kg ($k\gamma \geqslant 1.44$ m^2/kg) (Fig. 8). Re-entering occurs at $\gamma \geqslant 10$ m^2/kg, because the orbit pericenter enters the Earth's atmosphere.

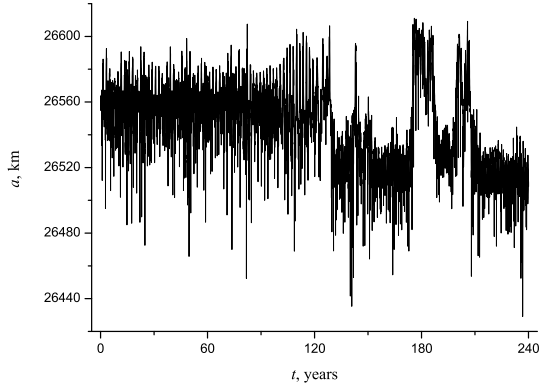Figure 8. *Evolution of the semi-major axis of the orbit a of the Molniya object ($a_0 = 26560$ km, $\gamma = 1$ m^2/kg).*

When moving along an orbit of the critical inclination $i \approx 63.4°$, the position of the orbit pericenter is saved since $\dot{g} \approx 0$. The resonance connected with the critical orbit inclination was observed at all the considered AMR values $\gamma = 0.001 - 9$ m^2/kg ($k\gamma = 0.00144 - 12.96$ m^2/kg) (Fig. 9, 10).
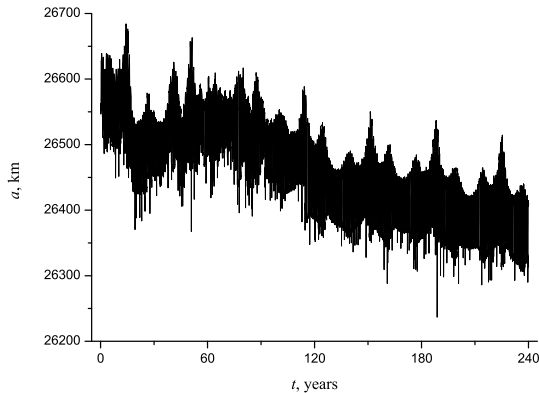

Figure 9. *Evolution of the semi-major axis of the orbit a of the Molniya object ($a_0 = 26560$ km, $\gamma = 8$ m^2/kg).*
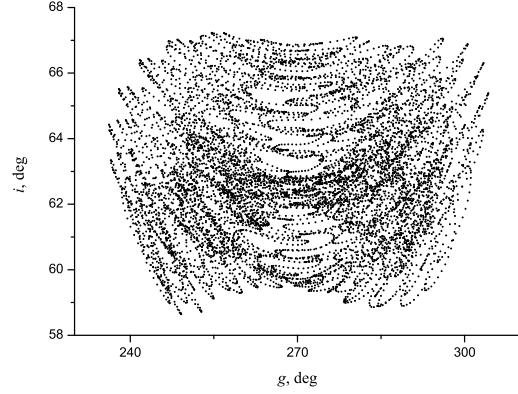

Figure 10. *Evolution of the inclination of the orbit i and the argument of the pericenter of the orbit g for the Molniya object ($a_0 = 26560$ km, $\gamma = 8$ m^2/kg).*

2.6. Region of 1:3 resonance for circular equatorial orbits

At low $\gamma \leqslant 0.01$ m^2/kg ($k\gamma \leqslant 0.0144$ m^2/kg), the initial values of the semi-major axis ensuring motion in the region of the 1:3 resonance are in the range from $20\,274\,655$ to $20\,274\,690$ m for n and i resonances, and from $20\,279\,005$ to $20\,279\,120$ m, for a e resonance. The amplitude of oscillations of the semi-major axis is 220 m in the zone of n and i resonances i.e., $a_{\min} = 20\,274\,650$ m and $a_{\max} = 20\,274\,870$ m (Fig. 11), and 200 m in the e resonance zone: from $a_{\min} = 20\,279\,000$ m to $a_{\max} = 20\,279\,200$ m.
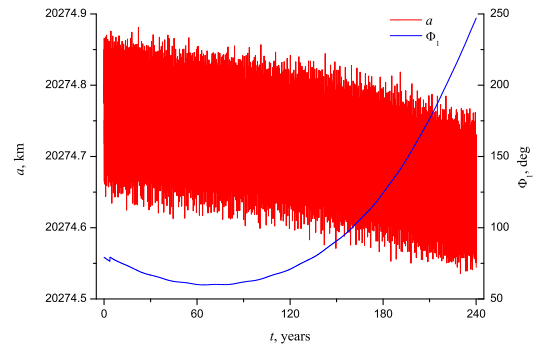
Figure 11. *Evolution of the semi-major axis of the orbit a and of the critical argument Φ_1 of a circular equatorial orbit in the region of the 1:3 resonance ($a_0 = 20274665$ m, $\gamma = 0.01$ m^2/kg).*

An increase in the AMR up to $\gamma \geqslant 0.02$ m^2/kg ($k\gamma \geqslant 0.0288$ m^2/kg) results in escape from the 1:3 resonance. One can conclude that the 1:3 resonance zone for circular equatorial orbits is very narrow and does not exceed

several hundred meters. Regions of n and i resonances overlap in the 1:3 resonance zone.

3. ESTIMATION OF SECULAR PERTURBATIONS OF SEMI-MAJOR AXIS

The light pressure effect, including accounting for the Poynting–Robertson effect, results in a secular increase in the semi-major axis of a spherically symmetrical satellite. This is manifested the most for objects with $\gamma \geqslant 1$ m^2/kg [14]. In resonance regions, the effect weakens significantly; however, the orbital evolution can change quantitatively if an object has a high AMR and moves near the boundary of a resonance zone.

The secular perturbations of the semi-major axis $\dot{\bar{a}}$ are extremely weak inside resonance zones and do not exceed several cm/year at $k\gamma \leqslant 1.44$ m^2/kg. Reliable estimates $\dot{\bar{a}}$ of can be obtained from the numerical simulation results only for trajectories passing near the boundaries of a resonance zone. The secular perturbations of the semi-major axis are $\dot{\bar{a}} = -10$ cm/year near the boundaries of the zone of libration of the 1:1 resonance ($a_0 = 42195$ km) at $k\gamma = 1.44$ m^2/kg.

The secular perturbations $\dot{\bar{a}}$ increase in absolute value modulus outside resonance zones with semi-major axis a. Thus, for a circular equatorial orbit at $\gamma = 1$ m^2/kg ($k\gamma = 1.44$ m^2/kg), the modulus of secular perturbations $|\dot{\bar{a}}|$ is 30 m/year for the initial value of the semi-major axis $a_0 = 20274$ km (the neighborhood of the 1:3 resonance), 50 m/year for $a_0 = 26600$ km (the neighborhood of the 1:2 resonance), and 80 m/year for $a_0 = 42300$ km (supergeosynchronous orbit). It is corresponded to [16].

4. ESTIMATION OF AMR OF SPACE OBJECTS FROM THE RESULTS OF POSITIONAL OBSERVATIONS

Positional observations of space objects moving in geosynchronous, supergeosynchronous, highly elliptical, medium-earth, and other orbits are carried out routinely at the Astronomical Observatory of the Ural Federal University using the Schmidt SBG telescope, four-axes mounted, with a primary mirror 500 mm in diameter, a focal length of 788 mm, and a correcting plate 425 mm in diameter.

An Alta U32 CCD camera is mounted at the prime focus of the telescope. It is equipped with 2184×1472 elements of 6.8×6.8 μm in size. The scale of an image received with the CCD system is $1.803''$/pixel; the system's field of view is $1.094° \times 0.737°$ [9].

During observations, the SBG telescope and the CCD system are controlled using the SBGControl software specially developed at AO UrFU [10].

The results of CCD observations of satellites are astrometrically processed at the SBG telescope using the FitsSBG software also developed at AO UrFU. The rms errors of the determination of satellite coordinates by intrinsic convergence of astrometric reduction are $0.1'' - 1''$. To improve the orbit elements and estimate the AMR, the Celestial Mechanics software, developed at the Astronomical Institute of the University of Bern [4], is used. For estimating AMR, an object is considered as a sphere, all points of which have an equal reflection coefficient k ranging from 1 to 2.

According to the results of positional observations for objects on high and medium orbits carried out at the SBG telescope in 2010–2012, the product $k\gamma$ has been estimated for high- and medium-orbit objects. AMR are detected from 0.011 to 0.175 m^2/kg for geosynchronous and supergeosunchronous objects and from 0.016 to 0.94 m^2/kg for Molniya type objects. The minimal time intervals required for reliable estimation of $k\gamma$, were 14 days for geosynchronous orbits, seven days for Molniya orbits, and five days for orbits in the neighborhood of the 1:3 resonance.

The estimates of $k\gamma$ can be related to small and moderate values. For geosynchronous and supergeosynchronous objects, the orbital evolution noticeably and quantitatively changes under the light pressure effect at $k\gamma \geqslant 1$ m^2/kg [12]. In Sections 2.3 – 2.6, we shown that the light pressure effect can result in significant qualitative changes in the orbital evolution of objects in neighborhood of the 1:2 and 1:3 resonances even at moderate AMR [14].

5. CONCLUSION

Widths of resonance zones decrease with an increase in AMR for circular equatorial orbits in the 1:1 and 1:2 resonances in the following sense. If one chooses an initial value of the semi-major axis different from the exact resonance value, the AMR at which escape from resonance occurs decreases (in comparison with the initial conditions corresponding to an exact resonance). Correspondingly, a maximally admissible range of oscillations of the semi-major axis at which an object maintains the resonance motion mode (in comparison with objects with low AMR) decreases. A noticeable reduction of a resonance region is observed at $\gamma \geqslant 1$ m^2/kg ($k\gamma \geqslant 1.44$ m^2/kg). Escape from the resonance mode for orbits with large inclinations occurs at $\gamma \geqslant 1$ m^2/kg; therefore, this effect is weakly manifested for non-equatorial and highly elliptical orbits.

Comparison of AMR values, at which resonance zones significantly reduce (for the 1:2 and 1:3 resonances) with estimates of AMR from the observation results, shows that the effect of low-order resonances on the long-term orbital evolution of objects with maximal AMR should significantly weaken. Further observations of these objects are of interest for revealing features of the orbital

evolution of space debris.

The possibility of transition between regions corresponding to secondary resonances in the 1:2 resonance zone, identified from numerical simulation results, is of practical interest. Highly accurate prediction of the motion of objects on similar orbits requires accurate accounting for non-gravitational perturbing factors. Calculation of the AMR of such objects from observational results is an urgent problem.

An decrease in the modulus of secular perturbations of the orbit semi-major axis a caused by the Poynting–Robertson effect with a increases the estimate of the time interval required for ground impact of an object with a high AMR. Objects with higher AMR have higher probabilities of passing through the regions of low-order resonances without temporal capture into resonance. However, an increase in secular perturbations of the orbit semi-major axis while approaching Earth slows down the process of clearing the near-Earth space of space debris.

ACKNOWLEDGMENTS

REFERENCES

1. Allan R.R., (1967). Resonance Effects due to the Longitude Dependence of the Gravitational Field of a Rotating Primary, *Planet. Space Sci.*, **15**(1), 53–76

2. Allan R.R., (1967). Satellites Resonance with the Longitude Dependent Gravity. II. Effects Involving the Eccentricity, *Planet. Space Sci.*, **15**(12), 1829–1845

3. Anselmo L. & Pardini C., (2009). Dynamical Evolution of High Area-to-Mass Ratio Debris Released into GPS Orbits, *Adv. Space Res.*, **43**(10), 1491–1508

4. Beutler G., (2005). *Methods of Celestial Mechanics*, Springer-Verlag, Berlin, Heidelberg, vol. 2

5. Bordovitsyna T.V., Baturin A.P., Avdyushev V.A. & Kulikova P.V., (2007). Numerical Model of Motion for Earth Artificial Satellite. New Version, *Izv. Vyssh. Uchebn. Zaved., Fiz.*, **50**(12/2), 60–65

6. Chao C.C., (2006). Analytical Investigation of GEO Debris with High Area-to-Mass Ratio, *AIAA Paper*, AIAA-2006-6514

7. Chao C.C. & Gick R.A., (2004). Long-Term Evolution of Navigation Satellite Orbits: GPS/GLONASS/GALILEO, *Adv. Space Res.*, **34**(5), 1221–1226

8. Gedeon G.S., (1969). Terrestrial Resonance Effects on Satellite Orbits, *Celest. Mech.*, **1**(2), 167–189

9. Glamazda D.V., (2012). SBG Camera of Kourovka Astronomical Observatory, *Astrophysical Bulletin*, **67**(2), 230–236

10. Glamazda D.V., (2012). Principal Algorithms for the Control of Kourovka Observatory SBG Camera, *Astrophysical Bulletin*, **67**(2), 237–244

11. Früh C. & Schildknecht T., (2012). Variation of the Area-to-Mass Ratio of High Area-to-Mass Ratio Space Debris Objects, *Mon. Notic. Roy. Astron.*, **419**(4), 3521–3528

12. Kuznetsov E.D., (2011). The Effect of the Radiation Pressure on the Orbital Evolution of Geosynchronous Objects, *Solar Syst. Res.*, **45**(5), 433–446

13. Kuznetsov E.D. & Kudryavtsev A.O., (2009). Accuracy of Long-Term Forecasting Geosynhronous Satellite Motion, *Russian Physics Journal*, **52**(8), 841–849

14. Kuznetsov E.D., Zakharova P.E., Glamazda D.V., et al., (2012). Light Pressure Effect on the Orbital Evolution of Objects Moving in the Neighborhood of Low-Order Resonances, *Solar Syst. Res.*, **46**(6), 442–449

15. Lemoine F.G., Kenyon S.C., Factor J.K., et al., (1998). *The Development of the Joint NASA GSFC and National Imagery and Mapping Agency (NIMA) Geopotential Model EGM96*, NASA/TP-1998-206861, NASA Goddard Space Flight Center, Greenbelt

16. Mignard F., (1982). Radiation Pressure and Dust Particle Dynamics, *Icarus*, **49**(3), 347–366

17. Mikisha A.M. & Smirnov M.A., (1997). The Influence of Solar Light Pressure to GEO Objects. Evolution Aspects, In *Proc. of the Second European Conf. On Space Debris* ESA SP-393, ESA Publications Division, European Space Agency, Noordwijk, The Netherlands, 323–325

18. Slabinski V.J., (1980). Poynting–Robertson Drag on Satellites Near Synchronous Altitude, *Bull. Amer. Astron. Soc.*, **12**, 741

19. Slabinski V.J., (1983). Poynting–Robertson Force Allowing for Wavelength-Dependent Reflection Coefficients and Non-Spherical Shapes, *Bull. Amer. Astron. Soc.*, **15**, 869

20. Smirnov M.A., Mikisha A.M., Novikova E.S. & Rykhlova L.V., (2001). Secular Variations of Semimajor Axis Of Debris Particles Near GEO due to Solar Radiation Pressure, In *Proc. of the Third European Conf. On Space Debris* ESA SP-473, ESA Publications Division, European Space Agency, Noordwijk, The Netherlands, 403–406

21. Sochilina A.S., (1982). On the Motion of a Satellite in Resonance with Its Rotating Planet, *Celest. Mech.*, **26**(4), 337–352

22. Valk S., Lemaître A. & Anselmo L., (2008). Analytical and Semi-Analytical Investigations of Geosynchronous Space Debris with High Area-to-Mass Ratios Influenced by Solar Radiation Pressure, *Adv. Space Res.*, **41**(7), 1077–1090